SWARM 2017: The 2nd International Symposium on
Swarm Behavior and Bio-Inspired Robotics
October 29-November 1, Kyoto, Japan

Bio-Inspired Design and Kinematic Analsyis of Dung Beetle-Like Legs

A. Kapilavai[1,2,*], J. Ignasov[1,2], K. Filonenko[3], J.C. Larsen[1], E. Baird[4], J. Hallam[1], S. Büsse [5], A. Kovalev[5], S.N. Gorb[5], L. Duggen[2] and P. Manoonpong[1,*]

[1] CBR Embodied AI & Neurorobotics Lab, The Mærsk Mc-Kinney Møller Institute, The University of Southern Denmark, Odense M, Denmark
[2]SDU Mechatronics, Mads Clausen Institute, The University of Southern Denmark, Sønderborg, Denmark
[3] Center for Energy Informatics, The Mærsk Mc-Kinney Møller Institute, The University of Southern Denmark, Odense M, Denmark
[4]Department of Biology, Lund University, Lund, Sweden
[5]Department of Functional Morphology and Biomechanics, Zoological Institute Christian-Albrechts-Universität zu Kiel, Kiel, Germany
(*E-mail:sakap15@student.sdu.dk, poma@mmmi.sdu.dk)

Abstract: The African dung beetle *Scarabaeus galenus* can use its front legs to walk and manipulate or form a dung ball. Its multifunctional legs have not been fully investigated or even used as inspiration for robot leg design. Thus, in this paper, we present the development of real dung beetle-like front legs based on biological investigations. Each leg consists of three main segments which were built using 3D printing. The segments were combined with in total four active DOFs in order to mimic locomotion and object manipulation of the beetle. Kinematics analysis of the leg was also performed to identify its workspace as well as to design its trajectory. To this end, the study contributes not only to novel multifunctional robotic legs, but also to the methodology of the bio-inspired leg design.

Keywords: Dung beetles, Locomotion, Object manipulation, kinematic control.

1. INTRODUCTION

To date, different types of insect-like walking robots have been developed [1-3]. Examples include the hexapod robots AMOS [1], HECTOR [2] and BILL-Ant [3] with 3-DOF legs, the hexapod robots LAURON V [4] and ASTERIS [5] with 4-DOF legs, and the hexapod robot WEAVER [6] with 5-DOF legs. While the 3-DOF legs enable the robots to walk on rough terrain [1-3] and to climb over a high obstacle [1], the kinematic redundancy in the 4- and 5-DOF legs can improve the robot maneuverability on more complex terrains [4-6]. However, all these leg structures have been mainly designed for locomotion. If other function, like object manipulation, is required, an additional active gripper or manipulator is installed [4] which, as a consequence, needs extra energy. Furthermore, the added component will increase the robot weight; thereby requiring more torque of the actuators of the legs.

In contrast to all these robots, the African dung beetle can use its legs to walk, manipulate or form a dung ball, and transport it (Fig. 1). Besides walking, the front legs are used mainly for manipulating and forming a dung ball (Fig. 1(a)), the middle legs for pushing the ball, and the hind legs for steering the ball (Fig. 1(b)). From this point of view, biomechanical structures of real beetle legs are a good template for developing multifunctional robotic legs. We have previously developed a dung beetle-like hind leg [7] and its motion control. In this study, we continue our work by investigating the front leg of the real beetle through μCT and video recordings. Afterwards, we use this biological investigation to design and develop multifunctional dung beetle-like front legs. Here we also analyze kinematics of the leg. This paper is organized as follows. In section 2, we introduce the methodology of the bio-inspired leg design. In section 3, we present kinematic analysis of the leg. In section 4, we show our experimental results on leg trajectories and joint movements generated by inverse differential kinematic control. This paper finishes in section 5 with discussion and conclusions.

2. BIO-INSPIRED DESIGN METHODOLOGY

To achieve a multifunctional robotic leg that can perform both locomotion and object manipulation, we investigated the front leg of the African dung beetle *Scarabaeus galenus* through video recordings and μCT scans. For video recordings, we filmed the dung beetle while manipulating and transporting a dung ball (see Fig. 1) and then analyzed the front leg movements frame by frame. This was done to observe the range of leg

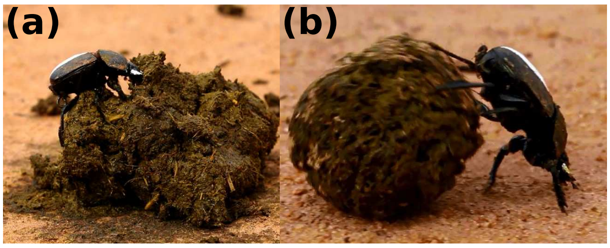

Fig. 1 The African dung beetle during (a) dung ball formation and (b) locomotion with the ball transportation (see Supplementary Video [8]).

† A.Kapilavai is the presenter of this paper.

movements.

In order to obtain kinematic details (including joint orientations and axes as well as the number of degrees of freedom (DOF)) of the front leg, we scanned the leg through a desktop μCT scanner (Skyscan 1172). The scanner captures x-ray images over a $360°$ rotation of the beetle. Based on these images, we reconstructed a 3D dataset that consists of a stack of virtual cross-section images through the entire specimen. Then we interactively segmented the parts of the leg from the dataset by assigning different labels to individual pixels within the stack of cross-sectional images. The segmented structures can then be visualized independently from the rest of μCT dataset and be exported as polygonal surfaces. Figure 2 summarizes the step by step of the bio-inspired design process.

Through the design process, we can identify three main segments of the leg, which include coxa, femur, and tibia with tarsus (Fig. 3(a)). There are three main active joints: TC-joint (connecting thorax and coxa), CT-joint (connecting coxa and trochanter+femur), and FT-joint (connecting trochanter+femur and tibia). Trochanter and femur segments are connected by a joint which allows very small movements; therefore, we simplified it as a fused component. The TC-joint is the most complex one which acts as a biaxial joint allowing for motions within two planes. Thus, we constructed this joint with two actuators that rotate around the y- and z-axes. The CT- and FT-joints are the simple ones which act as monoaxial joints allowing for motions within one plane each (Fig. 3(b)). Thus, we constructed each joint with one actuator that rotates around the x-axis. In total four actuators are used for the leg. Due to the actuator constraints, each segment of the leg was scaled 10 times from the original size. The size of each segment is approx. 26 mm for coxa, approx. 60 mm for femur, and approx. 100 mm for tibia with tarsus. The overall leg length including connections between segments is approx. 370 mm.

For the TC-joint, we used two HS-645MG servo motors where each of them can provide a torque of 1 N.m

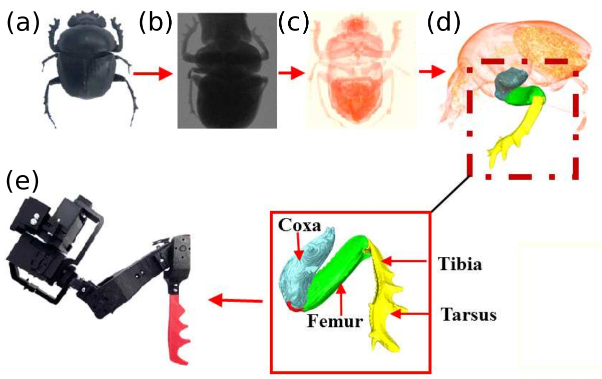

Fig. 2 (a) *Scarabaeus galenus* beetle (b) μCT scan of the beetle, (c) exoskeleton of the beetle, (d) after segmentation and reconstruction, (e) a dung beetle-like robotic leg.

and a speed of 0.0033 s/deg. For the CT- and FT-joints, we used two BMS-380MAX servomotors where each of them can provide a torque of 0.5 N.m and a speed of 0.0023 s/deg. All the servo motors are driven by a controller through the Multi-Servo IO-Board (Mboard). The Mboard is interfaced with a personal computer (PC) via RS232 serial connection at 57.6 kbits per second.

Taken together, the dung beetle-like front leg has the following characteristics:

1. The first motor q_1 of the TC-joint, rotating around the z-axis, moves the leg forward and backward.
2. The second motor q_2 of the TC-joint, rotating around the y-axis, can orient the leg downward mainly for object manipulation.
3. The third and fourth motors q_3 and q_4 for the CT- and FT-joints, rotating around the x-axis, are responsible for moving the leg toward or away from the body.
4. The length of the coxa segment is about 2 times and 3 times smaller than femur and tibia with tarsus segments, respectively.
5. The motors of the TC-joint require a high torque in order to move the entire leg, while the other two motors require a smaller torque since they move only the remaining leg excluding the coxa part.
6. All segments and connectors were 3D printed using purely PolyLactic Acid (PLA) thermo plastic, except the tibia with tarsus where we used a combination of PLA and a soft material (i.e. rubber) in order to obtain proper friction between the leg and the surface during locomotion and object manipulation.

3. KINEMATIC ANALYSIS

Here we present the kinematics of the 4-DOF dung beetle-like front leg (Fig. 3) in two parts: Forward kinematics using the Denavit-Hartenberg (DH) method and inverse kinematics using a differential kinematic method.

3.1. Forward Kinematics

The kinematic diagram of the leg with the coordinate frame assignment is shown in Fig. 4. The Denavit-Hartenbe (DH) parameters and the rotational ranges of all motors are listed in Table 1 and Table 2, respectively. (x_r, y_r, z_r) represents the reference frame, (x_b, y_b, z_b) the body frame, and (x_1, y_1, z_1) to (x_4, y_4, z_4) the lo-

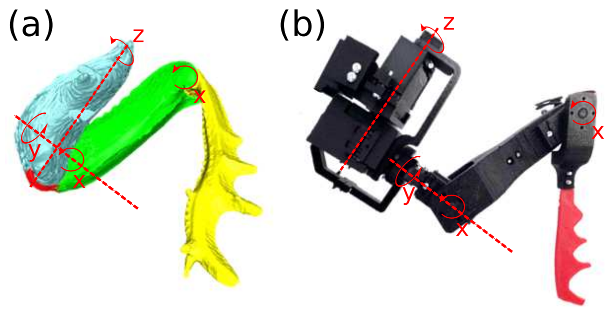

Fig. 3 (a) Dung beetle front leg. (b) the 4-DOF dung beelte-like front leg.

cal coordinate frames at the four motors respectively. (x_c, y_c, z_c) shows the local coordinate frame at the tip of the leg. The transformation matrix of the leg is described as:

$$T_{i+1}^{i} = Rot_{z,\theta_i} \cdot Trans_{z,d_i} \cdot Trans_{x,\alpha_i} \cdot Rot_{x,\alpha_i}$$
$$= \begin{bmatrix} c_{\theta_i} & -s_{\theta_i}c_{\alpha_i} & s_{\theta_i}c_{\alpha_i} & a_i c_{\theta_i} \\ s_{\theta_i} & c_{\theta_i}c_{\alpha_i} & -c_{\theta_i}s_{\alpha_i} & a_i s_{\theta_i} \\ 0 & s_{\alpha_i} & c_{\alpha_i} & d_i \\ 0 & 0 & 0 & 1 \end{bmatrix}, \quad (1)$$

where c_x and s_x denote $\cos(x)$ and $\sin(x)$ respectively.

$$T_c^1 = T_2^1 \cdot T_3^2 \cdot T_4^3 \cdot T_c^4 = \begin{bmatrix} n_x & o_x & a_x & p_x \\ n_y & o_y & a_y & p_y \\ n_z & o_z & a_z & p_z \\ 0 & 0 & 0 & 1 \end{bmatrix} \quad (2)$$

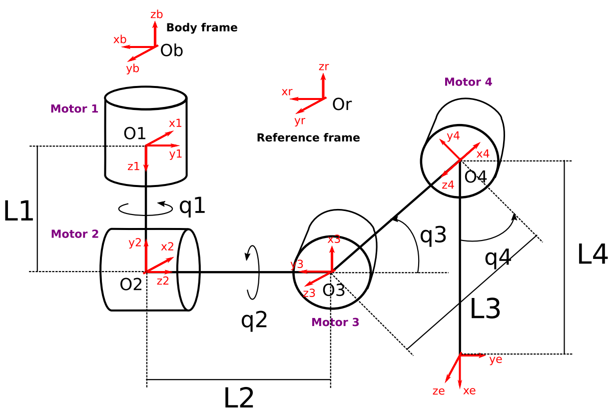

Fig. 4 Kinematic diagram of the leg configuration. Motor 1 (q_1) and Motor 2 (q_2) belong to the TC-joint. Motors 3 (q_3) and Motor 4 (q_4) belong to the CT- and FT-joints, respectively.

Table 1 Denavit-Hartenberg (DH) parameters for the dung beetle-like front leg.

Link	θ_i	d_i	α_i	a_i
Motor 1	q_1	L_1	$-\pi/2$	0
Motor 2	q_2	L_2	$-\pi/2$	0
Motor 3	q_3	0	0	L_3
Motor 4	q_4	0	0	L_4

Table 2 The ranges of motor joint angle limits of the robot.

Joint	$\mathbf{q_{min_i}}$	$\mathbf{q_{max_i}}$
Motor 1	$\frac{-\pi}{2}$	$\frac{\pi}{3}$
Motor 2	$\frac{3\pi}{4}$	π
Motor 3	$-\pi$	$\frac{\pi}{6}$
Motor 4	$\frac{2\pi}{3}$	$\frac{-\pi}{6}$

with c=$[p_x, p_y, p_z]^T$. Therefore, the position of the foot with respect to the global coordinate frame is given by:

$$\begin{aligned} p_x =& L_3(S_1S_3) - L_2(S_1) + L_4C_4(S_1S_3 + C_1C_2C_3) \\ &+ L_4S_4(C_3S_1 - C_1C_2S_3) + L_3(C_1C_2C_3), \quad (3) \\ p_y =& L_2C_1 - L_3C_1S_3 - L_4C_4(C_1S_3 - C_2C_3S_1) \\ &- L_4S_4(C_1C_3 + C_2S_1S_3) + L_3(C_2C_3S_1), \quad (4) \\ p_z =& L_1 - L_3(C_3S_2) - L_4(C_3C_4S_2) + L_4(S_2S_3S_4), \quad (5) \end{aligned}$$

where $(n_x, n_y, n_z)^T$, $(o_x, o_y, o_z)^T$, and $(a_x, a_y, a_z)^T$ are the orientation vectors of the foot tip.

3.2. Inverse Kinematics

We employed common closed-loop methods that are used for redundant robots [9]. The differential kinematics equation represents a linear mapping between joint angular velocities $[\dot{q}_1, \dot{q}_2, \dot{q}_3, \dot{q}_4]^T$ and foot tip velocities $[\dot{p}_x, \dot{p}_y, \dot{p}_z]^T$. Therefore, the differential kinematics equation can be described as:

$$\dot{\boldsymbol{x}}_e = \boldsymbol{v}_e = \mathbf{J}(\mathbf{q})\dot{\mathbf{q}}, \quad (6)$$

where $\boldsymbol{v}_e$ is here the $\mathbf{r} \times \mathbf{1}$ vector (r=3) of foot tip velocity for the specific task and $\mathbf{J}$ is the corresponding $(\mathbf{r} \times \mathbf{n})$ (r=3,n=4) **Jacobian** matrix, and $\dot{\mathbf{q}}$ is the $\mathbf{n} \times \mathbf{1}$ vector of joint velocities(n=4). Let

$$\boldsymbol{e} = \boldsymbol{x}_d - \boldsymbol{x}_e \quad (7)$$

be the expression of error, where $\mathbf{x_d}$ is the desired position and $\boldsymbol{x}_e$ is the actual position of the leg foot tip. The time derivative of Equation (7) is given by:

$$\dot{\boldsymbol{e}} = \dot{\boldsymbol{x}}_d - \dot{\boldsymbol{x}}_e. \quad (8)$$

According to differential kinematics, Equation (6) can be written as:

$$\dot{\boldsymbol{e}} = \dot{\boldsymbol{x}}_d - \mathbf{J}(\mathbf{q})\dot{\mathbf{q}}. \quad (9)$$

Notice that Equation (9) leads to an *inverse kinematics algorithm*, it is worth relating the computed joint velocity vector $\dot{\mathbf{q}}$ to the error $\boldsymbol{e}$ so that Equation (9) gives a differential equation describing error evolution over time. Nonetheless, it is necessary to choose a relationship between $\dot{\mathbf{q}}$ and $\boldsymbol{e}$ that ensures convergence of the error to zero. Having formulated inverse kinematics in algorithmic terms implies that the joint variables $\mathbf{q}$ corresponding to a given leg pose $\mathbf{x_d}$ are accurately computed when the error $\boldsymbol{x}_d - \boldsymbol{k}(\mathbf{q})$ as a function of $\boldsymbol{e}$ permits finding inverse kinematics algorithms with different features, where $\mathbf{k}$ indicates the forward kinematics. On the assumption that the $\mathbf{J}(\mathbf{q})$ is square matrix and non singular, the choice

$$\dot{\mathbf{q}} = \mathbf{J}^{-1}(\dot{\boldsymbol{x}}_\mathbf{d} + \mathbf{K}\boldsymbol{e}) \quad (10)$$

leads to the equivalent linear system

$$\dot{\boldsymbol{e}} + \mathbf{K}\boldsymbol{e} = \mathbf{0}. \quad (11)$$

Solution (11) can be generalized for the case of the redundant leg, which gives

$$\dot{\mathbf{q}} = \mathbf{J}^{*} \cdot (\dot{\boldsymbol{x}}_{\mathbf{d}} + \mathbf{K}\boldsymbol{e}), \tag{12}$$

where $\mathbf{J}^{*} = \mathbf{J}^{\mathbf{T}}(\mathbf{J}\mathbf{J}^{\mathbf{T}} + \lambda^{\mathbf{2}}\mathbf{I})^{-\mathbf{1}}$ and $\mathbf{K}$ is a positive definite, usually diagonal matrix, λ is the Lagrange multiplier and $\mathbf{I}$ is the identity matrix. In developed algorithm, desired target ($\boldsymbol{x}_d$) is constant, therefore, ($\dot{\boldsymbol{x}}_d$) is zero. So the final equation is

$$\dot{\mathbf{q}} = \mathbf{J}^{*} \cdot (\mathbf{K}\boldsymbol{e}). \tag{13}$$

The block diagram corresponding to the inverse kinematics algorithm given by Equation 13 is illustrated in Fig. 5.

4. EXPERIMENTAL RESULTS

Here we present three main experimental results: the workspace of the leg, the performance of the inverse kinematic control, and the trajectory planning of the leg for locomotion and object manipulation based on video recordings of the African dung beetle. All the results were verified by using the robotics toolbox in Matlab [10]. Figure 6(a) shows the workspace of the dung beetle-like front leg. Due to the second degree of freedom (q_2) of the TC-joint, the positions in the reachable workspace span an extensive volume. In contrast, if the degree of freedom is fixed where the leg becomes a 3-DOF robot leg, the workspace is reduced (Fig. 6(b)). This demonstrates that our bio-inspired leg design provides an extended workspace which is useful for object formation or manipulation, like the dung beetle.

To evaluate the performance of our inverse kinematic control, we let the leg tip follow a cubic polynomial trajectory. To do so, we set the leg at the initial orientation $q = [0,\ \pi/4,\ -\pi/4,\ \pi/3]^T$ rad where the corresponding initial position is $[15.2,\ 10.00,\ -13.2]^T$ cm. The end position $[7.6,\ 2.7,\ -7.6]^T$ cm is given as an input to the control. Intermediate positions are assigned with respect to the polynomial trajectory. Figure 7 shows the profiles of the joint positions $[q_1,\ q_2,\ q_3,\ q_4]^T$ and velocities $[\dot{q}_1,\ \dot{q}_2,\ \dot{q}_3,\ \dot{q}_4]^T$ that follow the polynomial trajectory. Note that the initial $\boldsymbol{v}_0$ and final $\boldsymbol{v}_f$ velocities are considered to be zero. Figure 8 shows the trajectory planning of leg movements for locomotion. From our observation of the front leg of a real dung beetle during locomotion, we realize that the movement of the leg tip can be simplified as an ellipse trajectory on the horizontal plane. Therefore, we used an ellipse equation:

$$\begin{aligned} x_{desired} &= 25.5 + \sin(\phi), \\ y_{desired} &= 1 - 5\cos(\phi). \end{aligned} \tag{14}$$

To generate this trajectory, the joint angle q_2 can be fixed. Thus for walking purpose, only 3 DOFs are sufficient and no redundancy is required.

For object manipulation, based on dung beetle video recordings, we observed the movement of the leg tip which can be simplified as an ellipse trajectory which lines in the horizontal and vertical planes. Therefore, we used the following ellipse equation:

$$\begin{aligned} x_{desired} &= 30 + \sin(\phi), \\ z_{desired} &= 5 + 2.5\cos(\phi). \end{aligned} \tag{15}$$

In this case, we can see that the redundancy is necessary for the task. Figure 9 shows the trajectory planning of leg movements for object manipulation.

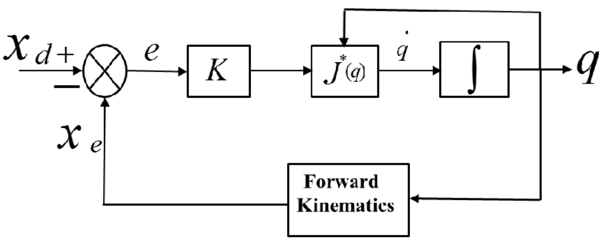

Fig. 5 Block diagram of inverse kinematic algorithm control for desired trajectory generation.

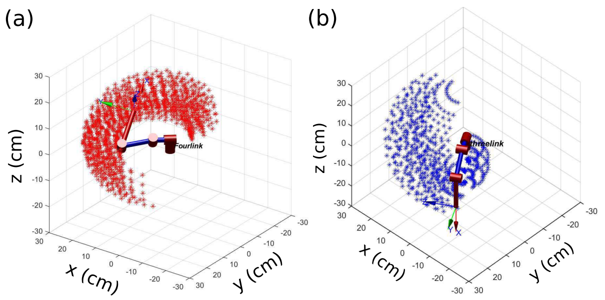

Fig. 6 The workspaces of (a) the 4-DOF dung beetle-like leg with a volume of 1375.036928 $\times 10^{-6} m^3$ and (b) the standard 3-DOF robot leg with a volume of 365.525875 $\times 10^{-6} m^3$.

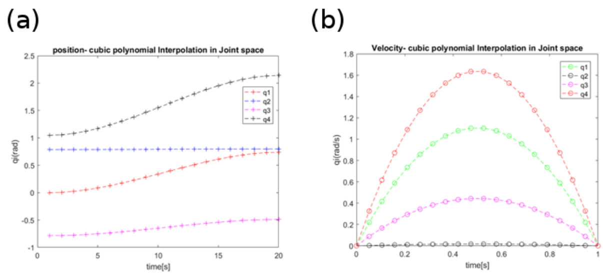

Fig. 7 Cubic trajectory to determine joint positions and velocities for the developed inverse kinematic algorithm control. (a) Joint positions. (b) Joint angular velocities.

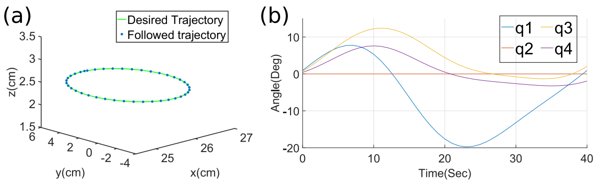

Fig. 8 (a) Simplified trajectory for locomotion and (b) corresponding joint angle variations.

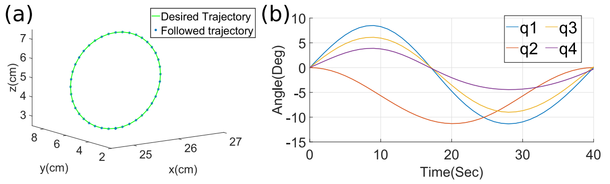

Fig. 9 (a) Simplified trajectory for object formation and (b) corresponding joint angle variations.

5. CONCLUSION

We presented a way of designing bio-inspired legs in a systemic way and outlined the design procedure, which is based on μCT scans of a real dung beetle. We used the data to construct the real dung beetle robot leg with 4 DOFs that allows for locomotion and object manipulation. We performed kinematic analysis where closed-loop methods were employed for solving the inverse kinematic problem of the leg. To check efficacy of the implemented inverse differential kinematic control, closed loop trajectories are generated in the joint and Cartesian spaces. Our experiments show that the use of additional DOF extends the workspace up to 73% , which makes our design applicable for performing multiple tasks in addition to a standard 3-DOF leg. Although our preliminary results shown here are based on one leg (i.e. right front leg), we have recently constructed the second front leg (i.e. left front leg), which is a mirror of the right leg. Figure 10 shows the CAD model of the setup for two legs. For future work, we will use the setup of the two front legs with an additional body joint to investigate object manipulation (e.g., forming a ball as a dung beetle does). We will also investigate dynamic motion control and implement muscle models [11] for joint compliance to achieve smooth and efficient locomotion and object manipulation behaviors.

ACKNOWLEDGEMENT

This research was supported by Centre for BioRobotics (CBR) at University of Southern Denmark (SDU, Denmark).

REFERENCES

[1] P. Manoonpong, U. Parlitz, F. Wörgötter. “Neural control and adaptive neural forward models for insect-like, energy-efficient, and adaptable locomotion of walking machines”, Front. Neural Circuits, Vol. 7, No. 12, DOI: 10.3389/fncir.2013.00012, 2013.

[2] A. Schneider, J. Paskarbeit, M. Schilling, J. Schmitz. “HECTOR, a bio-inspired and compliant hexapod robot”, In: Proceedings of the 3rd Conference on Biomimetics and Biohybrid Systems, Living Machines 2014, pp. 427–430, DOI: 10.1007/978-3-319-09435-9_51, 2014.

[3] W. A. Lewinger, R. D. Quinn. “Neurobiologically-based control system for an adaptively walking hexapod”, Industrial Robot, Vol. 38, No. 3: 258–263, DOI: 10.1108/01439911111122752, 2011.

[4] A. Roennau, G. Heppner, M. Nowicki, R. Dillmann. “LAURONV: A versatile six-legged walking robot with advanced maneuverability”, In: Proceedings of the 2014 IEEE/ASME International Conference on Advanced Intelligent Mechatronics (AIM), pp. 82–87, DOI: 10.1109/AIM.2014.6878051, 2011.

[5] K. Inoue, T. Tsurutani, T. Takubo, T. Arai. “Omnidirectional gait of limb mechanism robot hanging from grid-like structure”, In: Proceedings of IEEE/RSJ International Conference on Intelligent Robots and Systems (IROS), pp. 1732–1737, DOI: 10.1109/IROS.2006.282133, 2006.

[6] M. Bjelonic, N. Kottege, P. Beckerle. “Proprioceptive control of an over-actuated hexapod robot in unstructured terrain”, In: Proceedings of IEEE/RSJ International Conference on Intelligent Robots and Systems (IROS), pp. 2042–2049, DOI: 10.1109/IROS.2016.7759321, 2016.

[7] G. Di Canio, S. Stoyanov, J.C. Larsen, J. Hallam, A. Kovalev, T. Kleinteich, S.N. Gorb, P. Manoonpong. “A robot leg with compliant tarsus and its neural control for efficient and adaptive locomotion on complex terrains”, Artif Life Robotics, Vol. 21, No. 3: 274–281, DOI: 10.1007/s10015-016-0296-3, 2016.

[8] Supplementary Video, “www.manoonpong.com/DungBeetle/SGBeetle.wmv”.

[9] B. Siciliano, L. Sciavicco, L. Villani, G. Oriolo. “Robotics: Modelling, Planning and Control”, Springer-Verlag London, DOI: 10.1007/978-1-84628-642-1, 2009.

[10] P. I. Corke. “A Robotics Toolbox for MATLAB”, IEEE Robotics and Automation Magazine, Vol. 3, No. 1, pp. 24-32, 1996.

[11] X. Xiong, F. Woergoetter, P. Manoonpong. “Adaptive and Energy Efficient Walking in a Hexapod Robot under Neuromechanical Control and Sensorimotor Learning”, IEEE Transactions on Cybernetics, Vol. 46, No. 11: 2521–2534, DOI: 10.1109/TCYB.2015.2479237, 2016.

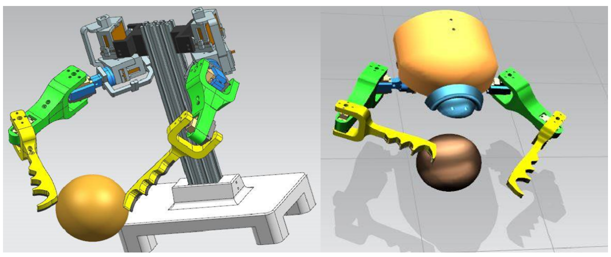

Fig. 10 CAD model of two front legs.